Arabian Journal of Chemistry (2023) **16**, 105061

King Saud University

Arabian Journal of Chemistry

www.ksu.edu.sa
www.sciencedirect.com

ORIGINAL ARTICLE

Anti-corrosion performance of dehydroacetic acid thiosemicarbazone on XC38 carbon steel in an acidic medium

Said Boukerche [a,b], Hana Ferkous [c,d,*], Amel Delimi [c,d], Amel Sedik [e], Amel Djedouani [f,g], Khadidja Otmane Rachedi [h], Hamza Bouchoukh [c], Malika Berredjem [h], Moussa Zahzouh [i], Abdelaziz Himour [i], Stefano Bellucci [j], Manawwer Alam [k], Yacine Benguerba [l,*]

[a] *Department of Material Sciences, Faculty of Science and Technology, University Mohamed Cherif Messaaadia of Souk Ahras, 41000, Algeria*
[b] *Laboratory of Surface Engineering (LIS), University Badji Mokhtar of Annaba, 23000, Algeria*
[c] *Laboratoire de Génie Mécanique et Matériaux, Faculté de Technologie, Université de Skikda, 21000, Algeria*
[d] *Département de Technologie, Université de Skikda, 21000 Skikda, Alegria*
[e] *Scientific and Technical Research Center in Physico-chemical Analysis, BP 384, Bou-ismail Industrial Zone, RP 42004, Tipaza, Algeria*
[f] *Laboratoire de Physicochimie Analytique et Cristallochimie des Matériaux Organométalliques et Biomoléculaires, Université Constantine 1, 25000 Constantine, Algeria*
[g] *Ecole Normale Supérieure de Constantine, Ville Universitaire Ali Mendjeli, 25000 Constantine, Algeria*
[h] *Laboratory of Applied Organic Chemistry LCOA. Synthesis of Biomolecules and Molecular Modelling Group. Badji-Mokhtar - Annaba University. Box 12. 23000 Annaba, Algeria*
[i] *Laboratory of Metallurgy and Materials Engineering (LMGM), University Badji Mokhtar of Annaba 23000, Algeria*
[j] *INFN-Laboratori Nazionali di Frascati, Via E. Fermi 00044, Frascati, Italy*
[k] *Department of Chemistry, College of Science, King Saud University, PO Box 2455, Riyadh 11451, Saudi Arabia*
[l] *Laboratoire de Biopharmacie Et Pharmacotechnie (LPBT), Ferhat Abbas Setif 1 University, Setif, Algeria*

Received 24 February 2023; accepted 3 June 2023
Available online 8 June 2023

* Corresponding authors at: Département de Technologie, Université de Skikda, 21000 Skikda, Alegria (Hana Ferkous).
E-mail addresses: h.ferkous@univ-skikda.dz (H. Ferkous), yacinebenguerba@univ-setif.dz (Y. Benguerba), yacinebenguerba@univ-setif.dz (Y. Benguerba).

Peer review under responsibility of King Saud University. Production and hosting by Elsevier.

Production and hosting by Elsevier

https://doi.org/10.1016/j.arabjc.2023.105061

KEYWORDS

Mild Steel;
Electrochemical tests;
Corrosion inhibition;
Schiff base DHATSC;
Inhibition efficiency;
DFT

Abstract Dehydroacetic acid thiosemicarbazone (DHATSC) was tested for its ability to suppress corrosion on mild steel XC38 (MS XC38) by measuring its effects by electrochemical impedance spectroscopy (EIS), weight loss (WL), and potentiodynamic polarization (PDP). Using weight loss tests and potentiodynamic polarization, the corrosion inhibiting efficiency (IE) of DHATSC for MS XC38 in 1.0 M HCl solution was calculated. The data showed that DHATSC was highly inhibitory, with increasing effectiveness as the inhibitor concentration increased. In 1 M HCl, the PDP curves showed that DHATSC was a mixed-type inhibitor. In addition to the EIS findings, the adsorption of DHATSC was also validated by analyzing the charge transfer resistance (Rct) values of the MS XC38 surface. At room temperature, the most outstanding corrosion inhibition efficiency as determined by weight loss was 78%; however, the PDP method obtained 94% at a concentration of 200 ppm. With a standard free energy (Gads) of −6.90 KJ.mol-1 for the adsorption stage, the Langmuir isotherm offered the most accurate description of DHATSC adsorption. The inhibitor has a nanocrystalline structure, measured by X-ray diffraction (XRD), with a mean crystallite size (D) of 56.11 nm. Scanning electron microscopy (SEM) and Fourier transform infrared spectroscopy (FTIR) analyses verified the mild steel's surface analysis. The theoretical calculations generally agreed with the experimental findings to a high degree.

1. Introduction

Steel and its numerous alloys are the metals most commonly used daily (Abd El-Lateef et al., 2016; Sedik et al., 2020; Kahlouche et al., 2022). Due to their high mechanical and physical properties, they are suitable for various applications, such as in the oil and gas industry, power generation, petrochemical plants, and civil engineering (Abd El-Lateef et al., 2016; Sedik et al., 2020; Kahlouche et al., 2022). Steel is widely used due to its accessibility, affordability, and resistance to various mechanical loads (Prajila et al., 2018; Belakhdar et al., 2020; Belakhdar et al., 2020; Ferkous et al., 2021). Rust, scale, and chalky deposits on carbon steel surfaces can be cleaned with hydrochloric acid, sulfuric acid, and nitric acid. However, acidic solutions will damage the cleaned carbon steel surfaces and initiate metallic corrosion due to their abrasive nature (Prajila et al., 2018; Belakhdar et al., 2020; Belakhdar et al., 2020; Ferkous et al., 2021). Corrosion is a natural process when metals are exposed to aggressive environments and undergo chemical reactions such as oxidation/reduction. Aggressive environments may vary, such as exposure to moisture, salt, and acid. This can lead to the deterioration of the metal structure, which can have significant economic and safety implications.

A variety of metals are affected by corrosion, including but not limited to steel, aluminum, and copper (Abd El-Lateef et al., 2016; Sedik et al., 2020; Kahlouche et al., 2022). Therefore, it is necessary to minimize the effects of corrosion by using various protection methods such as chemical dip coatings (DCC) (Al Zoubi et al., 2021; Al Zoubi et al., 2020) and the production of hybrid organic–inorganic (HOI) coatings on metal alloys by combining plasma electrolytic oxidation (PEO) and DCC methods (Al Zoubi et al., 2021; Al Zoubi et al., 2020), inhibitors, and design strategies (Boukerche et al., 2019; Belakhdar et al., 2021.). Corrosion is a chronic problem as metals revert to their natural state at the lowest energies, often resulting in chemical reactions with the environment. Even when metals are protected, the process can still occur over time. Additionally, corrosion can be difficult to manage as factors such as high temperature, humidity, and mechanical stress can cause it. Corrosive effects can be challenging to see, sometimes taking place in hard-to-reach areas or under protective coatings. Preventing and mitigating the impact of corrosion requires expertise, careful preparation, and maintenance. This may include selecting appropriate materials and coatings, establishing appropriate anti-corrosion systems, and maintaining and inspecting metal structures to detect and repair corrosion damage (Ibrahim et al., 2016; Delimi et al., 2022; Djellali et al., 2021).

Organic compounds can be used to reduce the effects of corrosion on metals (Miralrio and Espinoza Vázquez, 2020; Zerroug et al., 2018; Sedik et al., 2011; Sedik et al., 2014; Srivastava et al., 2017; Verma et al., 2018). Organic chemicals can be used in various ways to prevent metal corrosion. The use of organic paints or coatings as a barrier between the metal surface and the corrosive environment increases the corrosion resistance of metals. This is because they can be customized to provide specific chemical and physical properties, such as resistance to water, chemicals, or ultraviolet (UV) light (Miralrio and Espinoza Vázquez, 2020; Zerroug et al., 2018; Sedik et al., 2011; Sedik et al., 2014). Organic molecules can act as corrosion inhibitors by forming a coating at the metal-solution contact (Miralrio and Espinoza Vázquez, 2020; Zerroug et al., 2017; Sedik et al., 2011; Sedik et al., 2014). Other corrosion inhibitors have also been described in the literature, the addition of which to acid solutions is the best way to reduce acid attack. Several chemical families have been developed and used for this purpose for decades (Srivastava et al., 2017; Verma et al., 2018).

The interest of theoretical researchers in studying the chemical reactivity of inhibitors and the extent of interaction with metallic surfaces has recently increased (Suhasaria et al., 2020; Chugh et al., 2020; Singh et al., 2019; Haque et al., 2020). However, this research is particularly time-consuming for experimental approaches. Despite significant advances, the search for potent corrosion inhibitors remains strong. Studies have shown that molecular structure, chain length, functional groups, the presence of heteroatoms, and the particular electrolyte used impact the inhibitory properties of organic molecules toward metals (Suhasaria et al., 2020; Chugh et al., 2020; Singh et al., 2019; Haque et al., 2020). Researchers in this field have investigated using organic Schiff bases as potential carbon steel corrosion inhibitors to solve this problem, showing promising results in various challenging situations (Verma et al., 2018; Li et al., 2022; Sakthivel et al., 2020; Liu et al., 2018; Abd-ElHamid et al., 2023; Al-Gorair et al., 2023). Organic substances, called Schiff bases, have a carbon–nitrogen double bond with an imine functional group (El Batouti et al., 2023). Schiff bases are formed by the condensation reaction between an amine and an aldehyde or ketone (El Batouti et al., 2021). Numerous studies have been conducted on these compounds to determine if they can prevent corrosion in various materials, including carbon steel, under acidic conditions (Hossain et al., 2017; Sahu and Thakur, 2012).

The physisorption of heteroatoms such as Nitrogen, Sulfur, and Oxygen in the inhibitor's structure inhibits corrosion (Sahu and Thakur, 2012; Singh et al., 2011). Chemicals that form p-bonds and interact with the metal surface through their p-orbitals are highly effective inhibitors. Schiff bases' ''azomethane'' group (C = N) can inhibit or completely halt corrosion. Studies have shown that Schiff bases treated on steel (Ferkous et al., 2020; Abd El-Lateef et al., 2017; Abdelsalam et al., 2022; Al-Amiery et al., 2020; AltunbaşŞahin et al., 2020; Aouniti et al., 2016; Ashassi-Sorkhabi et al., 2005; Bedair et al., 2017; Boulechfar et al., 2021; Boulechfar et al., 2023; Messali et al., 2018), aluminum (Arjomandi et al., 2018; Yurt and Aykın, 2011; Aytac et al., 2005; Şafak et al., 2012; Naik et al., 2016) (ranging from 46% to 99.87% purity), and copper (Issaadi et al., 2014; Ehteshamzade et al., 2006; Zhang et al., 2016; Mishra et al., 2015; Mishra et al., 2015) exhibit high efficiency in resisting corrosion in acidic environments, with inhibition efficiency ranging from 87% to 99%.

The efficiency of 2-(2-methoxy benzylidene) hydrazine-1-carbothioamide (MBHCA) in preventing the corrosion of carbon steel in hydrochloric acid was studied, for example, by Ferkous et al. (Ferkous et al., 2020). At a concentration of just 200 ppm, adding MBHCA reduced corrosion by as much as 97.8 percent (ppm). MBHCA is believed to adsorb onto the steel surface and generate a protective layer, which is what provides the inhibition against corrosion. The functional groups of MBHCA connect to the metal surface by chemical bonding and electrostatic attraction, forming this protective layer.

Certain thiophene Schiff bases have been shown to inhibit carbon steel corrosion, with 91 and 97% efficiencies, respectively, as reported by Aouniti et al. (Aouniti et al., 2016) and Tezcan et al. (Tezcan et al., 2018). Researchers Liang et al. (Liang et al., 2019) showed that the 2-amino fluorene bis-Schiff base was nearly 100% efficient in preventing corrosion on carbon steel. Boulechfar et al. (Boulechfar et al., 2021) studied the influence of temperature on the corrosion rate and found that the Schiff base 2-furaldehyde semicarbazone had the most excellent inhibitory effect at 293 K. (FSC). However, the corrosion rate increased when the temperature was raised from 303 K to 323 K.

In another study, Zerroug et al. (Zerroug et al., 2021) investigated the anti-corrosion properties of Artemisia Herba alba (AHA) polyphenols. They found that the inhibition efficiency increased with temperature, ranging from 88.5% at 298 K to 92.9% at 323 K, with a concentration of 900 ppm. Belakhdar et al. (Belakhdar et al., 2020) examined an extract from Rosmarinus officinalis (RO) as a corrosion inhibitor for carbon steel. They observed greater effectiveness at lower temperatures, specifically in the 303 K to 333 K range, particularly with increased concentrations.

This research analyzes how well DHATSC protects mild steel from corroding in hydrochloric acid (HCl) solution. To determine the efficacy of the inhibitor, we used open circuit polarization (OCP) and potentiodynamic polarization (PDP) experiments with electrochemical impedance spectroscopy (EIS) and weight loss measures. The inhibitor's phase was determined via X-ray diffraction (XRD). Density functional theory (DFT) simulations were used to examine the behavior of molecules and electron interactions with the metal, and the adsorption parameters were also obtained. We compared theoretical results from quantum chemistry calculations and molecular dynamics simulations with actual data for a complete picture of the corrosion processes.

2. Materials and methods

2.1. Materials

2.1.1. Sample preparation for steel

Steel sheets with an iron content greater than 99.5% were used in the experiments. The relative proportions of the various chemical compounds are displayed in Table 1. The cylindrical models used in electrochemical tests had an exposed surface section of 0.27 cm^2, whereas samples for gravimetric studies and SEM analyses were (20 × 50 × 2) cm^3. Samples were cleaned in distilled water, washed with acetone to remove any grease, and then allowed to air dry before being polished with wet SiC paper (grade 220–2000). The powerful 1 M HCl solution was made using hydrochloric acid with a concentration of 37%.

Table 1 Elemental composition of MS XC38.

Element	C	Si	Mn	Al	P	S
(wt. %)	0.21	0.38	0.05	0.01	0.09	0.05

2.1.2. Working solutions

The strong electrolyte used in the experiments was diluting 37% hydrochloric acid (HCl) from analytical grade with 1 M distilled water. The effect of the inhibitor on the metal's corrosion behavior was studied by adding the inhibitor to the solution. We used inhibitor concentrations of both 200 and 60 ppm. Only double-distilled water was used in their preparation to guarantee the integrity of the test solutions.

2.2. Corrosion study

2.2.1. Gravimetric study

The corrosion rate (ν_inh) (g cm-2 h-1) after 6 h in a 1 M HCl solution, both with and without DHATSC inhibitor, can be measured using the following equation:

$$v_{inh} = (W_{initial} - W_{final})/(A * t) \quad (1)$$

Where: v_{inh} is the corrosion rate in grams per square centimeter per hour; $W_{initial}$ is the initial weight of the sample before exposure to the corrosive solution; W_{final} is the weight of the sample after 6 h of exposure; A is the surface area of the sample in square centimeters; t is the exposure time in hours.

The samples were cleaned and polished before being immersed in 1 M HCl solutions containing the inhibitor to obtain accurate results. After the 6-hour exposure period, the samples were washed with distilled water, degreased with acetone, dried, and weighed again. The difference in weight before and after exposure, divided by the surface area and exposure time, gives the corrosion rate in the presence and absence of DHATSC.

The following equation may determine the relative inhibitory efficiency compared to WL (IEwl).

$$IE_{wl} = \frac{W_{corr} - Wt_{corr}}{W_{corr}} \times 100 \quad (2)$$

The electrochemical and weight loss experiments were conducted three times as part of this investigation, and the obtained results exhibited a high level of reliability, with variances of only ± 1 to 2%.

2.2.2. Electrochemical measurements

EIS and PP experiments were performed using the Gamry framework on a standard three-electrode cell. MS XC38 electrodes were used to conduct investigations, while platinum electrodes served as counter electrodes and saturated calomel

electrodes (SCEs) were used as reference electrodes. We captured polarization curves at a rate of 0.5 mV.s^{-1}, with an open circuit potential (OCP) of −200 mV to + 200 mV.

Open-circuit potential EIS measurements were conducted using a frequency range of 100 kHz to 10 mHz and a peak-to-peak signal amplitude of 10 mV. The following formula was used to estimate the IE from PP Tests: (IE_{pdp}).

$$IE_{pdp} = \frac{i_{corr} - i'_{corr}}{i_{corr}} \times 100 \quad (3)$$

The substrate's current corrosion densities (i_{corr} and i'_{corr}) in 1 M hydrochloric acid (HCl) solution were measured in both the inhibitor's absence and presence. The corrosion densities were expressed in amperes per square centimeter (A.cm^{-2}).

The interfacial behaviors are described not by a perfect capacitor but by a constant phase element (CPE). The impedance of a CPE may be calculated using the following equation:

$$Z_{CPE} = \frac{1}{Q(jw)^a} \quad (4)$$

The CPE exponent "a" varies between 0 and 1, representing the deviation from ideal capacitive behavior. The CPE magnitude is denoted as "Q," and "w" indicates the angular frequency. Although the CPE is considered to approximate a perfect capacitor, it still accounts for any non-ideal characteristics present in the system.

The EIS defined IE_{EIS} is calculated as follows:

$$IE_{EIS} = \frac{R_{ct} - R'_{ct}}{R_{ct}} \times 100 \quad (5)$$

The measurements of charge transfer resistances, Rct and R'ct, were made with and without an inhibitor.

$$C_{dl} = \frac{\varepsilon\varepsilon_0 A}{d} \quad (6)$$

where A is the electrode's projected surface area, is the medium's dielectric constant, and ε_0 is free space's permittivity (8,854 × 10^{-14}F.cm^{-1}).

2.2.3. Characterization of surfaces

2.2.3.1. Fourier transforms infrared (FTIR) spectroscopy. The inhibitor's functional groups were identified using attenuated total reflection. The Fourier transform infrared spectroscopy attenuated total reflection technique was utilized. The ATR-FTIR data was collected using a Perkin Elmer Frontier spectrophotometer from 4000 to 400 cm^{-1}.

2.3. SEM analyses

The thermoscientific Quattro model scanning electron microscopy (SEM) was used to study the XC 38 steel' surface morphology. Depending on whether or not 200 ppm of DHATSC inhibitor was added, materials were immersed in 1 M hydrochloric acid at 298 K for 24 h.

2.4. Molecular modeling

For further analysis, the DMol3 module for Material Studio 2017 TM was used to run theoretical simulations on the experimental corrosion data. The geometry of DHATSC was optimized with the help of the GGA-BP86 functional, which used a double numerical basis (DNP). The inhibitors' chemical reactivity with steel was investigated by using theoretical characteristics.

$$\text{Chemical potential}\mu = -\chi = (E_{HOMO} + E_{LUMO})/2 \quad (7)$$

$$\text{global hardness}\eta = (-E_{HOMO} + E_{LUMO})/2 \quad (8)$$

$$\text{electrophilicity index}\omega = \frac{\mu^2}{2\eta} \quad (9)$$

$$\Delta N = \frac{\chi_{F_e} - \chi_{inh}}{2(\eta_{F_e} + \eta_{inh})} \quad (10)$$

The constant N represents the rate at which electrons move from the inhibitor to the steel surface. It is common practice to express the energies of molecular orbitals using their highest occupied (EHOMO) and lowest unoccupied (ELUMO) values. The χ_{Fe} value is 4.82 eV, while the η_{Fe} value is 0 (Pearson et al., 1992; Sedik et al., 2022).

Fukui indices (f_k^- and f_k^+) were determined to assess local activity:

$$f_k^- = \rho_N - \rho_{N-1}(electrophilicattack) \quad (11)$$

$$f_k^+ = \rho_{N+1} - \rho_N(nucleophilicattack) \quad (12)$$

The electronic densities are ρ_N(atom), ρ_{N+1}(anion) and ρ_{N-1}(cation).

For the adsorption energy, we have:

$$E_{ads} = E_{inh-steel} - (E_{inh} + E_{steel}) \quad (13)$$

Solubilization of the inhibitors in water was investigated using the Conductor-like Screening Model for Real Solvents (COSMO-RS) (Behloul et al., 2022; Bououden et al., 2021). Concurrently, the Adsorption module (Sun et al., 1998) in Material Studio 2017TM was utilized to study the inhibition using Metropolis Monte Carlo simulations (MCS) (Frenkel et al., 1996; Nakhli et al., 2020). The MCS technique finds the adsorbate/adsorbent pair with the lowest free energy. Simulations were conducted to study the process of DHATSC adsorption onto a steel surface, with the size of the containers determined by the number and types of molecules being stored. The "Dreiding" force field was utilized during the simulation to evaluate the strength of the molecular interactions.

3. Results and discussion

3.1. Synthesis

The Preparation of DHATSC involves the reaction of an equal-molar mixture of (0.01 mol) of dehydroacetic acid and thiosemicarbazide.

Dehydroacetic acid (1) (1.68 g) and thiosemicarbazide (2) (2.41 g) were combined to react in a mixture of pure ethanol (30 ml) and distilled water (10 ml). For three hours, the mixture was refluxed while being stirred. Using distilled water for washing and filtering afterward, the product was allowed to cool at room temperature before being deposited as a yellowish crystalline substance. A combination of (methanol/water) (60/40) produced yellow parallelepipedic crystals appropriate for XRD investigation (Scheme 1).

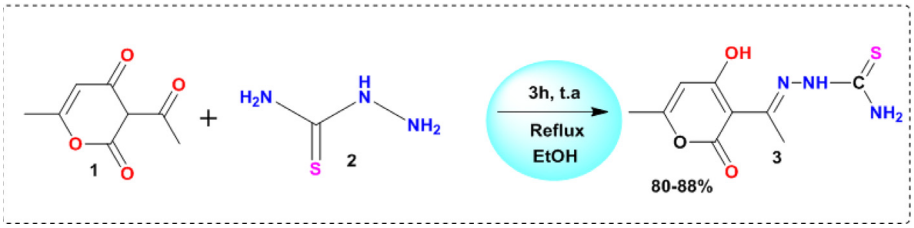

Scheme 1 Synthesis of 2-(1-(4-hydroxy-6-methyl-2-oxo-2H-pyran-3-yl) ethylidene) hydrazine-1 carbothioamide 3.

3.2. Fourier transform infrared (FTIR) spectra

Utilizing FTIR analysis, the structure of the produced chemical was determined. (Fig. 1), ^{1}H NMR (Fig. 2), and ^{13}C NMR (Fig. 3).

The FT-IR spectra of DHATSC showed several characteristic bands: the bands at 3300 and 3100 cm^{-1} correspond to the stretching vibrations of the two amine groups (N–H) and (NH_2); the band at 1685 cm^{-1} represents the stretching vibration of the azomethine group (C = N); the band at 1541 cm^{-1} corresponds to the stretching vibration of the carbon–carbon double bond (C = C); the band at 1415 cm^{-1} indicates the stretching vibration of the carbon–oxygen bond (C-O); the band at 1177 cm^{-1} represents the stretching vibration of the triazole group (N-N); the band at 1027 cm^{-1} corresponds to an intense stretching vibration of the carbon–sulfur bond (C-S); and the band at 603 cm^{-1} corresponds to the vibration of the Furan ring (Abdelsalam et al., 2022).

Specific signals in the 1H NMR spectra confirmed the formation of the pyrano-thioureas compound 3. A signal of around 3.25 ppm was observed for the NH proton, indicating the formation of the pyrano-thioureas compound. Additionally, a singlet signal at 10.5 ppm corresponded to the OH group, and two singlet signals between 2 and 2.5 ppm were related to the two methyl groups.

Moreover, data from the ^{13}C NMR spectra of the product further confirm the proposed structure with the appearance of signals attributable to the pyrane cycle between 160 and 180 ppm, C_4 at 180 ppm, and thioureas C_{14} at 178 ppm.

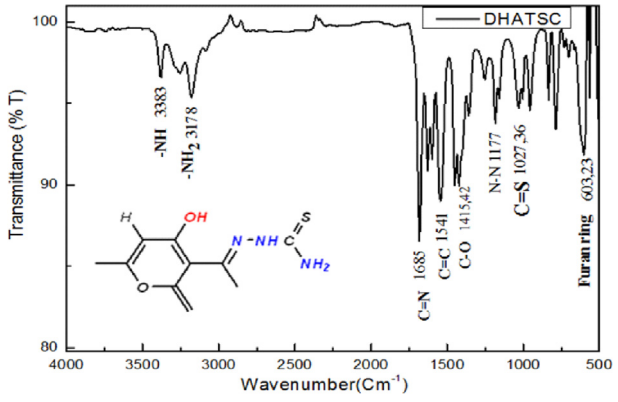

Fig. 1 FT-IR spectra of the synthesized Schiff base (DHATSC) inhibitor.

3.3. X-ray diffraction pattern

X-ray diffraction pattern reveals the nanocrystalline structure of DHATSC, which is demonstrated by intense peaks at 10.52° and 25.87° Fig. 4 is an XRD pattern showing that DHATSC has mostly a polycrystalline structure. System analysis indicates that the sample's precise arrangement is influenced by the compound's nature (molecular structure) and the synthesis circumstances. (Leontie et al., 2018). Fig. 4 shows the DHATSC molecule's XRD pattern, revealing its mostly polycrystalline structure. An analysis of the sample's molecular structure showed that it was affected by both the experimental circumstances of synthesis and the intrinsic properties of the molecule (molecular structure). Polycrystalline molecules' structure, development, electrical transport, and spectral features are highlighted. The chemical's XRD data show that crystal orientation preference already exists at the earliest stages of molecule formation. Debye-equation Scherrer's was used to get the average crystallite size (D):

$$D = \frac{k.\lambda}{\beta.coscos\theta} \tag{14}$$

- The Scherrer constant for spherical crystallites with cubic symmetry: k = 0.94
- The angular full-width at half-maximum of the XRD peak in radians: β = 0.15173
- The Bragg diffraction angle: θ = 12.93522°
- The wavelength of the incident X-ray beam: $\lambda_{Cu,\ K\alpha}$ = 1.54182 Å

Based on these parameters, the usual approach for structural analysis was used to determine the value of a type parameter, which was found to be D = 56.11 nm.

3.4. Gravimetric measurements

The corrosion rate of carbon steel and the efficacy of DHATSC as a corrosion inhibitor were calculated after extensive testing; the results are shown in Fig. 5. Mass loss of the metal was determined at 298 K after being immersed in HCl solutions at several concentrations with and without the inhibitor DHATSC.

The corrosion rate and the efficacy of the IE_{wl} corrosion inhibition approach are summarized in Table 2 from the WL trials.

MS XC38 loses weight when immersed in a blank sample, but the WL decreases as DHATSC concentration rises in the corrosive solution (Ferkous et al., 2020).

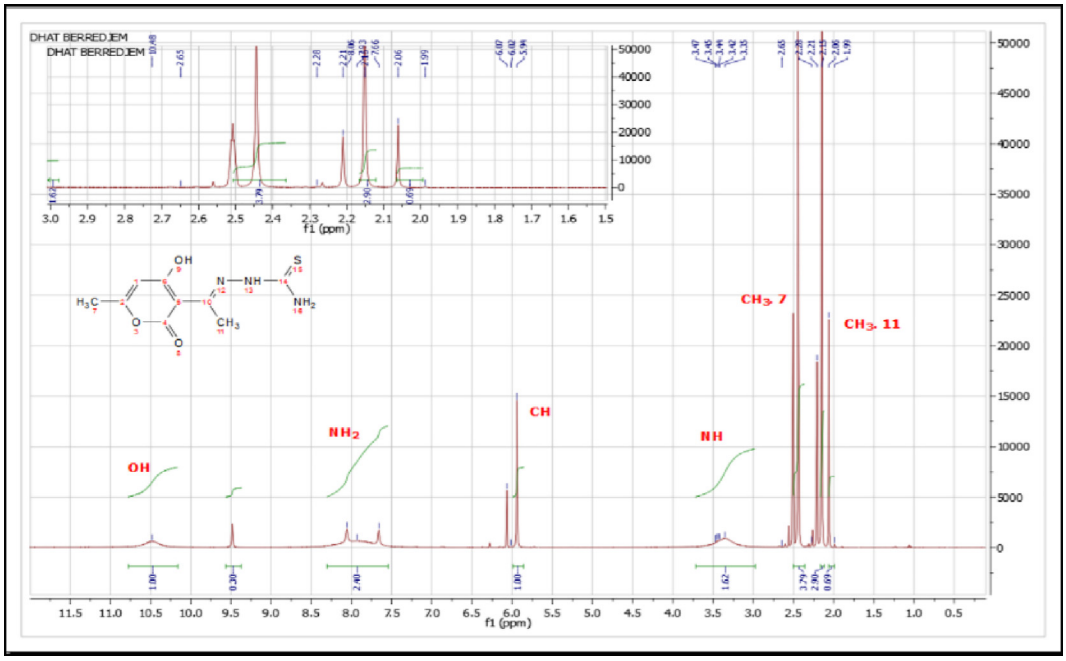

Fig. 2 ^{1}H NMR Spectra of DHATSC.

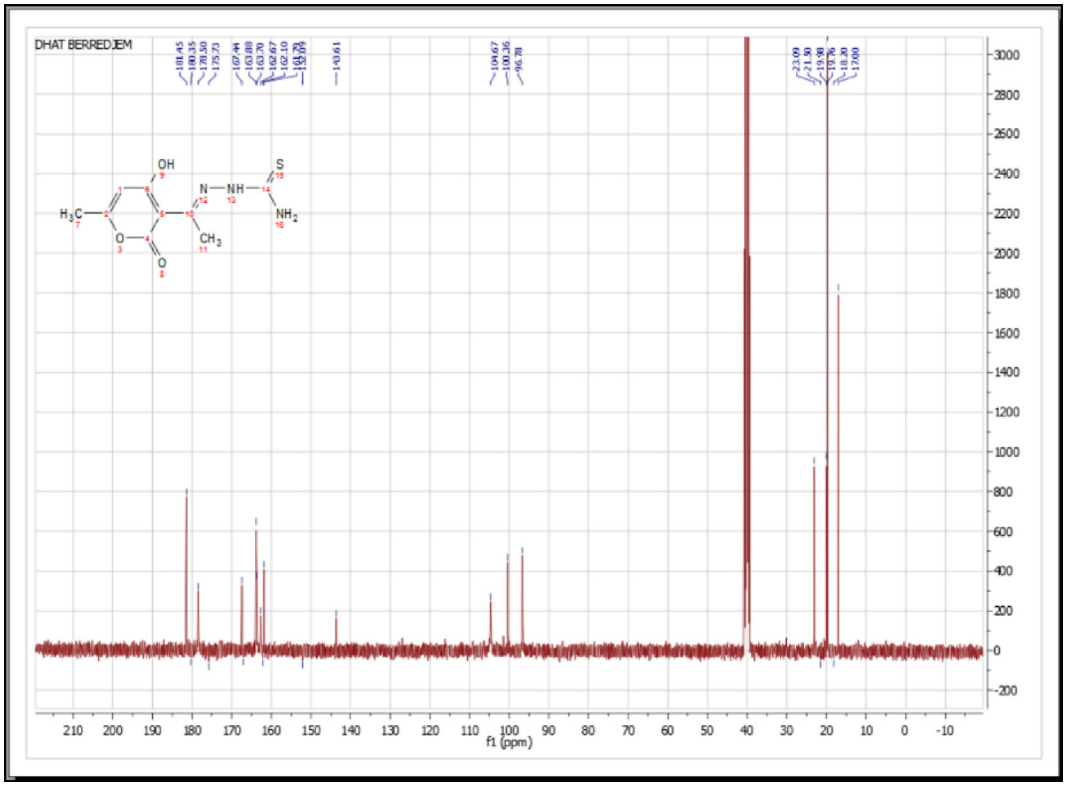

Fig. 3 ^{13}C NMR Spectra of DHATSC.

At a maximum effective concentration of 200 ppm, DHATSC exhibits an inhibition efficacy of 95.7%, which remains consistent. The corrosion protection provided to the steel is significant, with an inhibition efficacy of over 60% even at a minimal applied concentration of 60 ppm. The adsorption behavior of molecules in the presence of 1 M HCl is believed to be responsible for the corrosion inhibition mechanism of carbon steel. This mechanism involves molecules' adsorption on

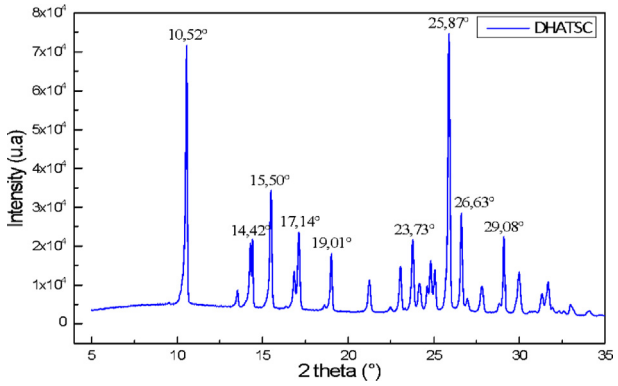

Fig. 4 DRX configuration of DHATSC.

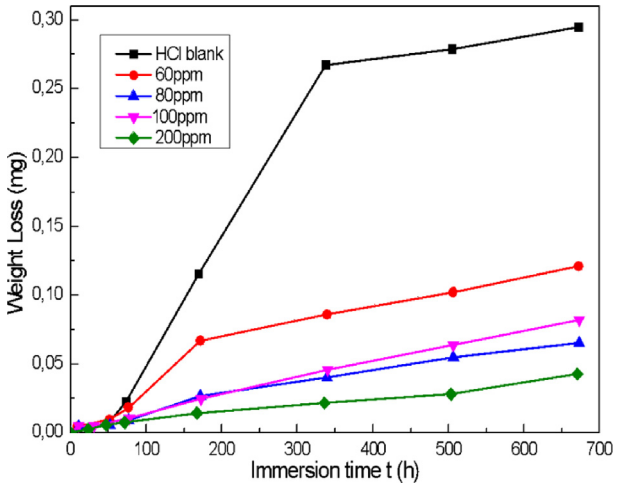

Fig. 5 Changes in steel sample mass loss as a function of immersion time, with and without DHATSC.

Table 2 Prevention of corrosion of XC38 MS in HCl solution at 298 K with varying DHATSC concentrations.

C(ppm)	Δm(g) ± SD	W.10^{-5} (mg.cm^{-2}.h^{-1})	E%
HCl	0.2685 ± 0.00050	6.15	–
60 ppm	0.08399 ± 0.00072	1.92	68.78
80 ppm	0.0588 ± 0.00025	1.35	78.05
100 ppm	0.043 ± 0.00050	0. 984	84
200 ppm	0.0119 ± 0.00008	0.2675	95.7

the steel's surface, effectively blocking active corrosion sites and reducing the overall corrosion rate (Arjomandi et al., 2018; Yurt and Aykın, 2011).

The overall results suggest that DHATSC effectively reduces the corrosion rate of the steel sample in a hydrochloric medium, which aligns with similar findings reported in previous studies on other Schiff bases (Boulechfar et al., 2021). Inhibitors play a crucial role in protecting carbon steel from corrosive acidic solutions by forming a protective layer on the metal surface. An inhibitor's electron-donating substituents enhance its effectiveness in inhibiting corrosion (Leontie et al., 2018; Chugh et al., 2020).

3.5. Evaluation of open circuit potential (OCP)

Time-dependent shifts in the open circuit potential (Eocp) provide valuable information about the initiation and progression of corrosion in mild steel (MS) and the relative significance of anodic and cathodic processes. It is widely accepted that achieving a steady-state open circuit condition is essential for conducting reliable electrochemical experiments. When MS is exposed to a harsh environment, the initial indication of degradation is a change in the measured free potential during a corrosion test. Fig. 6 illustrates the relationship between XC38 OCP and immersion time in a 1 M HCl solution across various inhibitor concentrations. Other research studies have observed similar trends (Khamis et al., 2013; Azooz and Kamal, 2019). Over time, when immersed in an uninhibited solution, the OCP gradually decreases. Subsequently, it experiences minimal fluctuations and reaches a nearly constant level within the recorded time frame. This activity indicates a passive layer forming on the substrate's surface (Solomon and Umoren, 2016; Ferkous et al., 2022). In contrast, the inhibited solution exhibits a different response. These interfaces appear to possess higher corrosion resistance (Heakal et al., 2018; Hsissou et al., 2021) since the Eocp shifts towards more positive potential values, and no significant variation in Eocp is observed throughout the measurement period.

3.6. Polarization measurements

The electrochemical investigation of MS with and without DHATSC yielded the polarization graphs shown in Fig. 7. Inhibitor addition has little influence on the anodic and cathodic curves, as can be seen by comparing the two. Table 3 is an updated list of electrochemical parameters.

Fig. 7 shows that MS has an Ecorr of −0.436 V for the Ag/AgCl reference electrode when immersed in the corrosive solution without an inhibitor. Activation regulates the increase in anodic and cathodic current densities due to anodic and cathodic overpotentials, respectively.

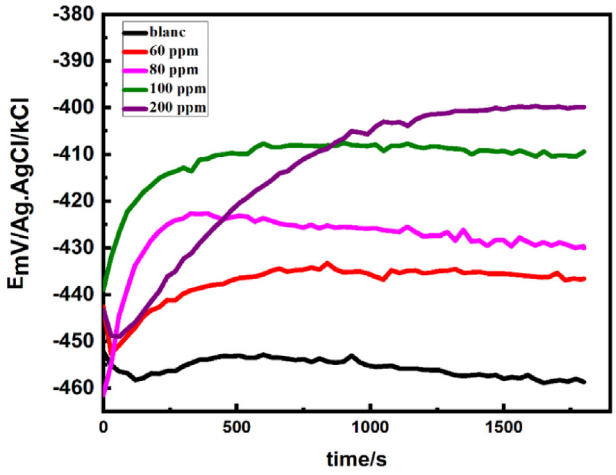

Fig. 6 Measurement of open-circuit potential in MS with and without DHATSC.

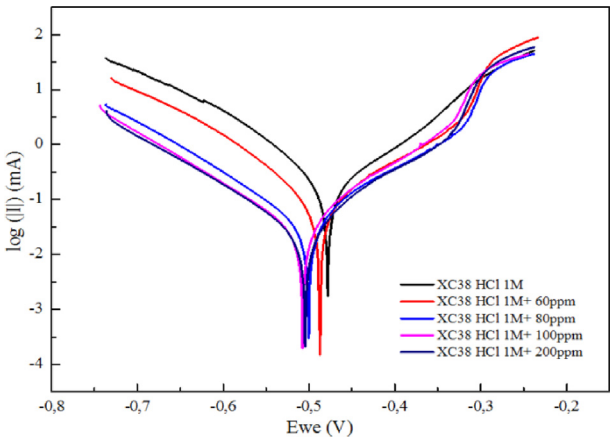

Fig. 7 XC38 steel polarization curves in 1 M HCl solutions.

Adding DHATSC to corrosive fluid reduces the anode and cathode's current density, increasing the corrosive medium's cathodic potential. Corrosion inhibitors are thus of the mixed type (Sedik et al., 2022; de Britto Policarpi and Spinelli, 2020).

Since the level of corrosion in a steel sample is directly related to the current density values, this finding demonstrates that DHATSC significantly reduces the deterioration of steel in 1 M HCl. Due to the corrosion inhibitor's presence, the anodic and cathodic branches of the inhibited solution curve altered to lower current densities than the blank system curve. At 200 ppm of inhibitor, the current density drops from 150 $A.cm^{-2}$ without inhibitor to 23 $A.cm^{-2}$ with inhibitor. Table 4 shows that when DHATSC concentration increases, corrosion current density drops and IE rises. These outcomes are consistent with the theory that inhibitor molecules attach to the metal surface, block active sites, and strengthen the metal's corrosion resistance (Sedik et al., 2020; Ferkous et al., 2021; Sedik et al., 2022; Solmaz et al., 2011). After this time, the IE % has decreased by 84%, and the protection is strengthened at greater concentrations, suggesting that including DHATSC in the corrosive environment protects the metal from dissolving.

3.7. Electrochemical impedance spectroscopy (EIS)

Electrochemical Impedance Spectroscopy (EIS) is a trusted non-destructive method for studying the electrical response of electrochemical systems, such as corrosion. Including charge transfer at the conductive electrode, adsorption, dissolution, and diffusion of charged species provides a thorough understanding of surface processes at the interface. Since EIS is non-destructive, the integrity of the metal/solution contact may be maintained during the analysis of these processes (Kaya et al., 2023). To examine the behavior of the surface inhibitor coating and the interface between the corrosive solution and XC 38 carbon steel, EIS was employed. A comparison of the EIS curves obtained with and without DHATSC reveals a distortion in the shape of the capacitive loop, particularly at its center. Fig. 8 presents the Nyquist and Bode plots obtained experimentally for MS samples after immersion for one hour in 1 M HCl solution, both with and without varying concentrations of DHATSC. This distortion in the curve shape can be attributed to frequency dispersion arising from non-homogeneity, impurities, and surface roughness on the carbon steel, which are well-known factors that influence the deviation from the ideal semicircular shape typically observed in solid electrodes (Saifi et al., 2019).

A capacitive loop with a wider diameter than the blank solution appears when DHATSC is present, suggesting that the impedance of the carbon steel has increased thanks to the assimilation of the inhibitor into the corrosive environment. Semi-circle diameters grew larger with increasing corrosive medium DHATSC concentrations, indicating a concentration-dependent mechanism by which DHATSC improves charge transfer resistance (Ferkous et al., 2017). Since the inhibitor raises the metal's resistance to corrosion, greater semi-circles in the Nyquist plots indicate more effective corrosion inhibition. The metal-electrolyte interface is characterized by a double electric layer, which can be altered in structure or composition when a new chemical species is introduced, such as an inhibitor. Anti-corrosion inhibitor adsorption may be studied by comparing the double-layer capacitance before and after the inhibitor was added (Boulechfar et al., 2023). A comparable circuit model was built using the experimental data to comprehend the Nyquist plots better. The resistances of the solution (Rs), the charge transfer (Rct), and the final film product are all accounted for in this model (Rp). Frequency dispersion due to the steel's roughness or non-homogeneity causes the depressed capacitive loops in the Nyquist charts. This model describes these loops using the constant phase element (CPE) rather than the double-layer capacitance. In the corrosion sector, the usage of CPEs in equivalent circuits is well acknowledged. Microscopic material features, including local charge inhomogeneity, surface defects, and dynamic electrochemical processes, are all considered by these CPEs, which affect the macroscopic resistance values.

The following equation can describe the impedance of CPEs:

Table 3 DHATSC, polarization parameters for XC38 steel corrosion in 1 M HCl.

	i_{corr}(μA.cm^{-2})	E_{corr}(mV)	β_a(mV)	β_c(mV)	CR (mmpy)	R_p (Ω.cm^2)	IE(%)
Blank	150.03	−436.55	76.5	85.8	1.54	172	–
60 ppm	41.07	−490.41	93.4	118.9	0.40	554	72.63
80 ppm	31.26	−516.84	85.5	96.3	0.28	630	79.16
100 ppm	42.69	−471.83	77.3	105.7	0.36	455	71.55
200 ppm	23.92	−504.44	76.5	98.0	0.19	781	84.56

Table 4 EIS measurements results.

	Rs (Ω)	Qdl (μF)	ndl	Rf (Ω)	Qf (μF)	nf	Rct (Ω)	IE %
XC38 HCl 1 M	1.042	2978	0.86	/	/	/	26.68	/
XC38 HCl 60 ppm	0.849	2.735	0.76	0.17	2241	0.7	220.4	87.71
XC38 HCl 80 ppm	1 0.973	81 0.29	0 0.81	158 0.7	320 8	1	255 0.4	89.55
XC38 HCl 100 ppm	1.924	55.52	0.81	81.3	409	0.95	313.6	91.78
XC38 HCl 200 ppm	1.221	5.625	0.0.60	13.67	641.2	0.73	462.1	94.22

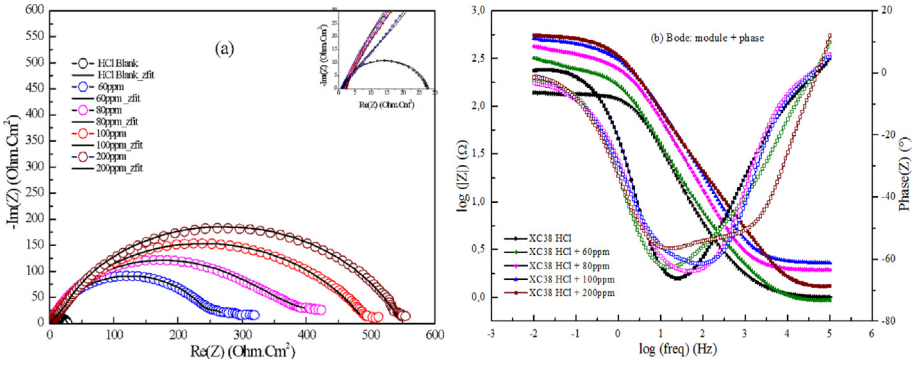

Fig. 8 EIS curves on MS XC 38 in 1 M HCl solutions with various amounts of DHATSC: a) Nyquist plots, b) Bode plots.

$$Z_{CPE} = \frac{1}{\gamma_0 (jw^n)} \tag{15}$$

Z_{CPE} stands for the impedance of a constant phase element (CPE), where γ_0 and n are the magnitude and exponent of the impedance. The frequency is expressed in hertz as $\omega = 2\pi f$, where j is the imaginary unit. The test findings suggest that the inhibitor stays on the metal's surface to form a barrier that prevents further corrosion. The solution's dielectric constant is decreased because this protective layer increases the thickness of the electric double layer. Solution resistance (RS), charge transfer resistance (Rct), diffuse layer resistance (Rd), and the constant phase element of the double-layer circuit are shown in Fig. 9. (CPE_{dl}).

The electrochemical data from the EIS experiments with DHATSC added is shown in Table 6.

Protection is maximized when the protective component's concentration is below 200 ppm. The enhanced protective efficacy of DHATSC molecules shows they work by adsorbing onto the metal surface of the solution to produce a protective layer. At high inhibitor concentrations, the value of IE is remarkably steady but somewhat lower than in the absence of inhibitors. The surface's porosity might be to blame for this drop. After the inhibitor was introduced, CPE values dropped dramatically.

Furthermore, these values continued to decrease with a rise in DHATSC concentration, showing that the produced inhibitor molecules were adsorbed onto the metal surface. Reduced capacitance (Verma et al., 2018; de Britto Policarpi and Spinelli, 2020) was achieved by increasing the coverage and/or thickness of the inhibitor's coating at the substrate/solution interface through adsorption. We have provided a summary table in our paper to help readers better grasp the events at the metal/solution interface. Table 5 shows that the double layer capacity (Cdl) and corrosion current density (i_{corr}) decrease. Concurrently, measurements show a rise in charge transfer resistance (Rct) and polarization resistance (Rp).

C_{dl} levels are decreased more noticeably when the inhibitor is present than when it is absent. Capacitance is significantly reduced, especially at increasing inhibitor efficiency levels, until the optimum is reached because the adsorbed inhibitor molecules displace water molecules inside the double layer. As a result, the dielectric constant decreases where the metal and solution meet as a protective coating develops on the metal surface (Boulechfar et al., 2023).

3.8. Impact of immersion time on the corrosion inhibition performance of the studied inhibitor

immersion time's impact on the studied inhibitor's corrosion inhibition performance was examined. Immersion tests were conducted for an optimal immersion time of 28 days at 25 °C, simulating acid cleaning operations. According to the data obtained from potentiodynamic polarization measurements (Fig. 10), the inhibition efficiency (IE%) of DHATSC increased with longer immersion times, ranging from 1 day to 21 days, and reached its highest levels at 200 ppm, ranging from 75.20% to 95.87% (see Table 6).

Table 6 exhibits how the system's corrosion resistance has been enhanced and highlights the ability of DHATSC molecules to prevent corrosion. This is evident as the polarization resistance (Rp) increased with longer immersion times in the DHATSC-inhibited solution, and even after 21 days, there was no decrease in Rp. These results collectively indicate the formation of a robust protective surface layer. The prolonged

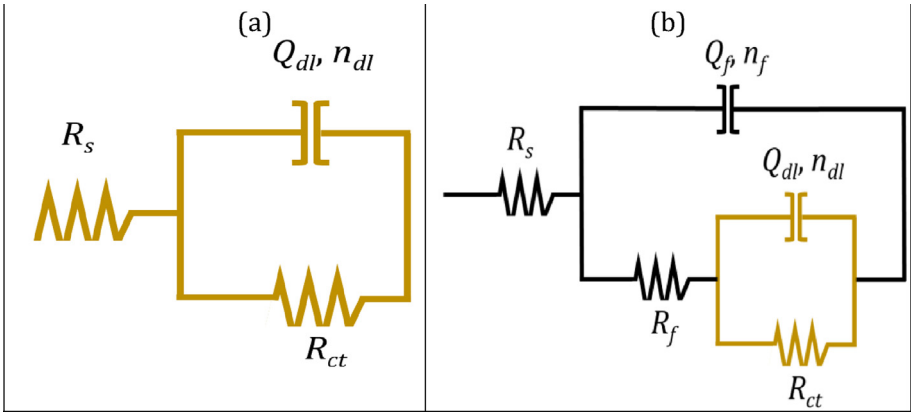

Fig. 9 Electrical Equivalent circuit.

Table 5 Comparison of corrosion test values.

	i_{corr}(μA.cm^2)	R_{ct}(Ω.cm^2)	C_{dl}(F.cm^2)	R_p(Ω.cm^2)	IE(%)
Blank	150.03	26.68	119.31	172	/
60 ppm	41.07	220.4	14.44	554	87.71
80 ppm	31.26	255 0.4	12.46	630	89.55
100 ppm	42.69	313.6	10.26	455	91.78
200 ppm	23.92	462.1	6.89	781	94.22

Table 6 Tafel parameters for MS in 1 M solution with 200 ppm of DHATSC after different immersion times.

	HCl	1 day	3 days	7 days	14 days	21 days	28 days
E_{corr} (mV)	−411.42	−477.94	−474.70	−459.18	−477.087	−453.53	−455.84
i_{corr}(μA.cm^{-2})	305.30	106.27	58.84	91.611	30.805	10.277	8.32
R_p (Ω.cm^2)	80.60	325.0	525.00	657.00	1936.00	1706.0	1145.0
EI(%)	–	75.20	84.64	87.732	92.961	95.275	89.91

immersion period allows DHATSC monolayers to adhere more effectively to the surface of mild steel, creating a more uniform and tightly-knit protective layer.

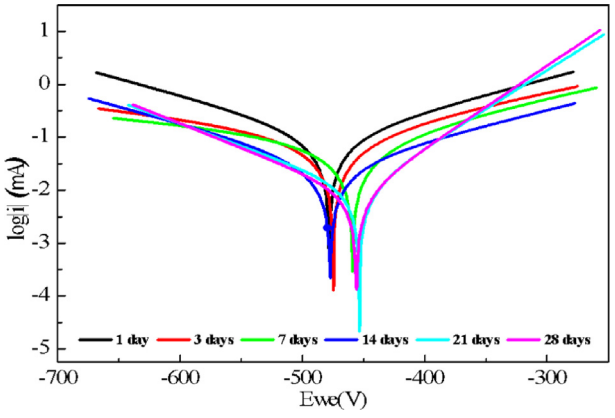

Fig. 10 Immersion time effect on Tafel plots of the interface mild steel/ HCl 1 M + 200 ppm of DHATS.

Fig. 11**(a)** represents the Nyquist diagrams for mild steel at different immersion times in the presence of DHATSC. The results showed that the immersion time influences the form and the size of the impedance spectra and, therefore, the corrosion inhibition efficiency of the inhibitor. Two capacitive loops appear. The first semi-circle is generally due to the high-frequency charge transfer phenomenon. And the second loop is related to the formation of the protective layer.

Immersion time was increased (1 to 21 days), and the impedance's diameter increased, suggesting an improvement of a capacitive surface film which promotes the protective film formation on the steel surface. It can also be seen from the Bode phase plots (Fig. 11(b)) that two relaxation time constants can describe the mild steel corrosion process in HCl media. They are ascribed to the charge transfer, electrical double-layer capacitor relaxation, and the adsorbed inhibitor molecules relaxation process.

3.9. Adsorption isotherm

The effectiveness of organic compounds in preventing metal corrosion is typically attributed to their adsorption onto the

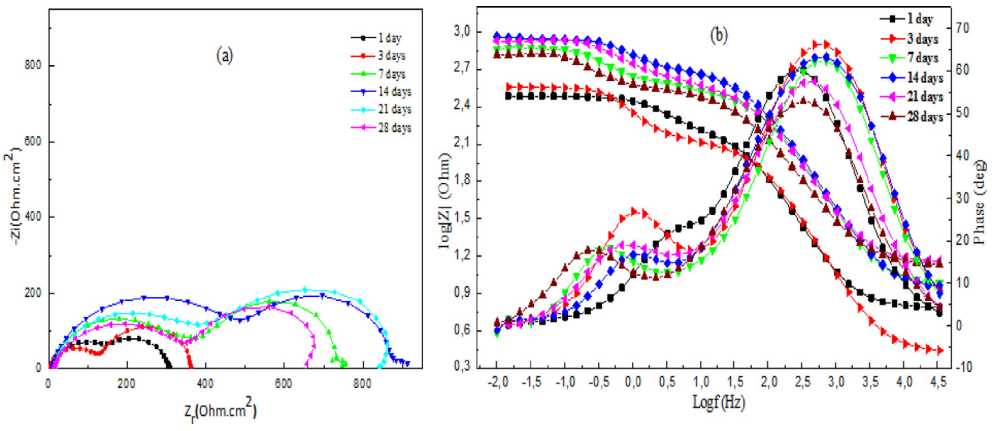

Fig. 11 Nyquist and Bode plots of mild steel in 1 M HCl with 200 ppm of DHATSC after different immersion times.

metal surface, effectively blocking susceptible areas from corrosion. Surface coverage refers to the ratio of occupied sites by the adsorbed inhibitor molecules to the total number of sites per surface unit. Analyzing adsorption isotherms helps establish a correlation between the metal surface coverage and the concentration of adsorbed species in the liquid phase at equilibrium, enabling a better understanding of the interaction between the inhibitor molecule and the steel surface. The inhibition of metal corrosion by organic compounds is generally linked to their ability to adsorb onto the metal surface and hinder corrosion-prone areas. Investigating adsorption isotherms facilitates the analysis of the interaction mechanism between the inhibitor molecule and the steel surface.

The gravimetric test results are utilized to determine the values of "θ" for different solutions of DHATSC in 1MHCl at equilibrium conditions.

$$\theta = \frac{E_{Wcorr}}{100} \tag{16}$$

The inhibition efficiency, E_{Wcorr}, is calculated using Eq. (16). Different isotherm models are used to establish the variations of θ with respect to DHATSC concentrations. Fig. 12 displays the plot of the selected isotherm model, which exhibits straight lines with high correlation coefficients close to unity. The fitting results yield coefficient of determination, R2, values of approximately 0.99, as determined by the following formula:

$$\frac{C_{inh}}{\theta} = \frac{1}{K_{ads}} + C_{inh} \tag{17}$$

The Langmuir constant, Kads, represents the equilibrium constant for the Langmuir adsorption isotherm. C_{inh} refers to the equilibrium inhibitor concentration in the liquid phase. The use of Langmuir adsorption isotherm indicates that it adequately describes the adsorption of DHATSC on the XC38 steel surface. The Kads values are utilized to evaluate the standard free energy, $\Delta G°_{ads}$, of the adsorption step, as expressed by the following equation:

$$\Delta G^{\circ}_{ads} = -RTln(55.5K_{ads}) \tag{18}$$

The value of K_{ads} is determined to be 3.08×10^{13} M^{-1}, and the corresponding $\Delta G°_{ads}$ is found to be -6.90 kJ·mol^{-1}. The negative value of ΔG°ads indicates that the adsorption of the inhibitor molecules onto the metal surface is spontaneous and exhibits strong binding. Moreover, the significant magnitude of $\Delta G°_{ads}$ (> -40 kJ·mol^{-1}) suggests that this adsorption can be classified as chemisorption, involving solid forces between the inhibitor molecules and the charged ions on the metal surface (Belakhdar et al., 2020; Singh et al., 2019).

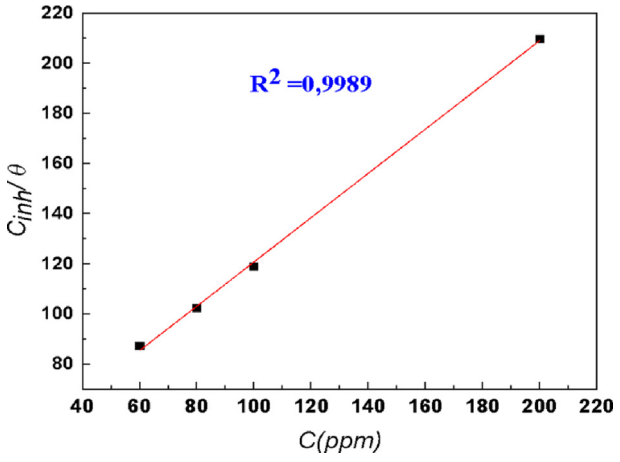

Fig. 12 Isotherm model plots for mild steel in 1 M HCl at various concentrations of DHATSC: Langmuir isotherm.

3.10. Surface characterization

The surface of MS XC38 was examined using SEM after exposure to test solutions, with and without 200 ppm DHATSC. Fig. 13(a) displays a micrograph of the MS surface in 1 M HCl, revealing extensive damage characterized by cracks, pits, and corrosion products due to the interaction with Cl- ions (Ferkous et al., 2019; Ferkous et al., 2018). In contrast, Fig. 13(b) shows a considerably smoother MS surface when the aggressiveness of the medium was significantly reduced, preventing corrosion. Upon adding DHATSC at a concentration of 200 ppm to the corrosive medium, Fig. 13(c) depicts a noticeable alteration with pits and fractures filling up. The molecules of Schiff bases in DHATSC appear to form a protective coating on the steel surface, resulting in a denser and more uniform coverage, thereby improving overall quality.

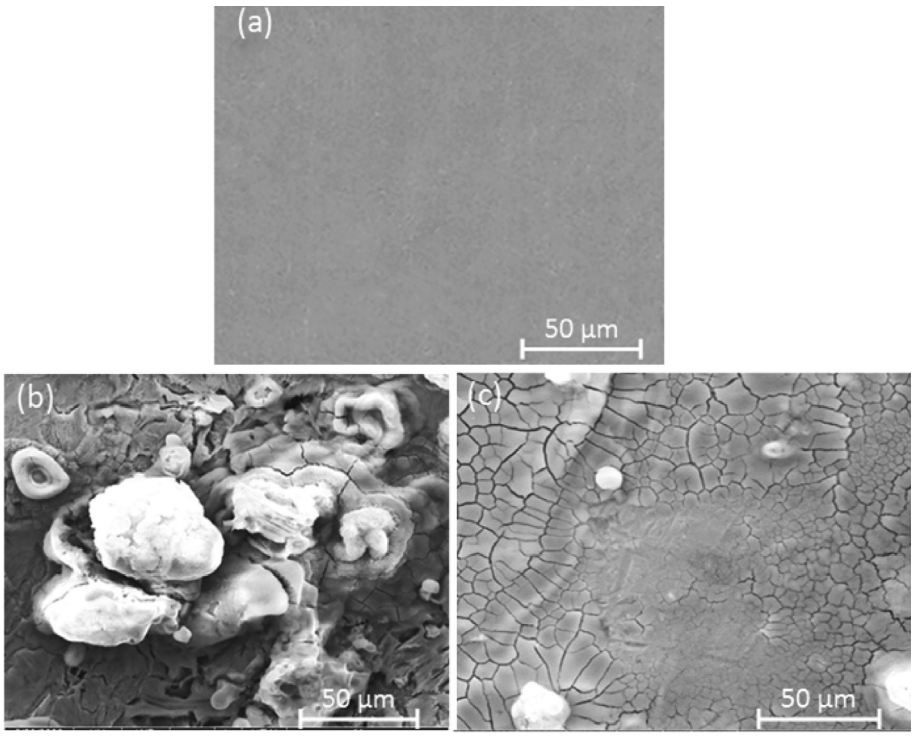

Fig. 13 SEM images of the carbon steel surface: **a)** before immersion in HCl, **b)** after immersion in HCl without DHATSC, and **c)** after immersion in HCl and 200 ppm DHATSC.

Figure 14 presents the results of the EDS analysis conducted on mild steel surfaces. The EDS spectra show a significant increase in the peaks corresponding to carbon (C), nitrogen (N), and sulfur (S) on the mild steel surfaces after corrosion in 1 M HCl solution containing DHATSC. This observation indicates the adsorption of DHATSC onto the surfaces of mild steel, leading to enhanced levels of C, N, and S (Li et al., 2022).

3.11. Quantum chemical study

3.11.1. Geometric optimizations

DFT optimized the investigated molecule's molecular structure using the B3LYP/6-31G (d,p) approach (Chugh et al., 2020; Radjai et al, 2018). Gaussian 09 (Haque et al., 2020) and the molecular visualization tool Gauss view (Al-Gorair et al., 2023) was used in both vacuum and solvent for all computations (DMSO). The HOMO, LUMO, and Egap energies were determined from these optimal structures. Fig. 15 displays the optimized DHATSC in DMSO.

The descriptors, energy level (HOMO, LUMO), gap energy, total energy, and linear polarizability (α_{Tot}) calculated by the DFT method, using B3LYP / 6-31G (d,p) in a vacuum and solvent DMSO are reported in Table 7.

The molecular sample that was under study has the smallest gap value. It is, therefore, less stable and more reactive in a vacuum. The acquired data show that this molecule's total energy (E) in DMSO is lower than in a vacuum, confirming that it is stable in DMSO.

3.11.2. Frontier molecular orbitals analysis

Fig. 16 shows this molecule's HOMO and LUMO frontier molecular orbitals in vacuum and DMSO (Boulechfar et al., 2021; Boulechfar et al., 2023). The frontier molecular orbital representation indicates that the LUMO orbital in DMSO is distributed throughout the entire molecule.

3.11.3. Chemical reactivity

- **Global reactivity parameters**

Other metrics that reflect the molecule's stability, such as electronic affinity, electronegativity, electronic potential, molecular hardness, and softness as the electrophilicity index, can be determined using the calculated energy levels (HOMO and LUMO) (Haque et al., 2020; Li et al., 2022). These equations can be used to calculate these parameters. (Table 8):

The obtained values are reported in Table 9.

The results reveal that the molecule in a vacuum has the lowest hardness value, which confirms that it is less stable and more reactive.

- **Local reactivity parameters**

Fukui indices

The Local reactivity descriptors, such as Fukui functions f^- predict a molecule's electrophilic and nucleophilic attack.

It is noted that the Fukui function, f^+, expresses the reactivity when a nucleophilic reagent attacks the molecule. In contrast, the Fukui function f^- gives information about the

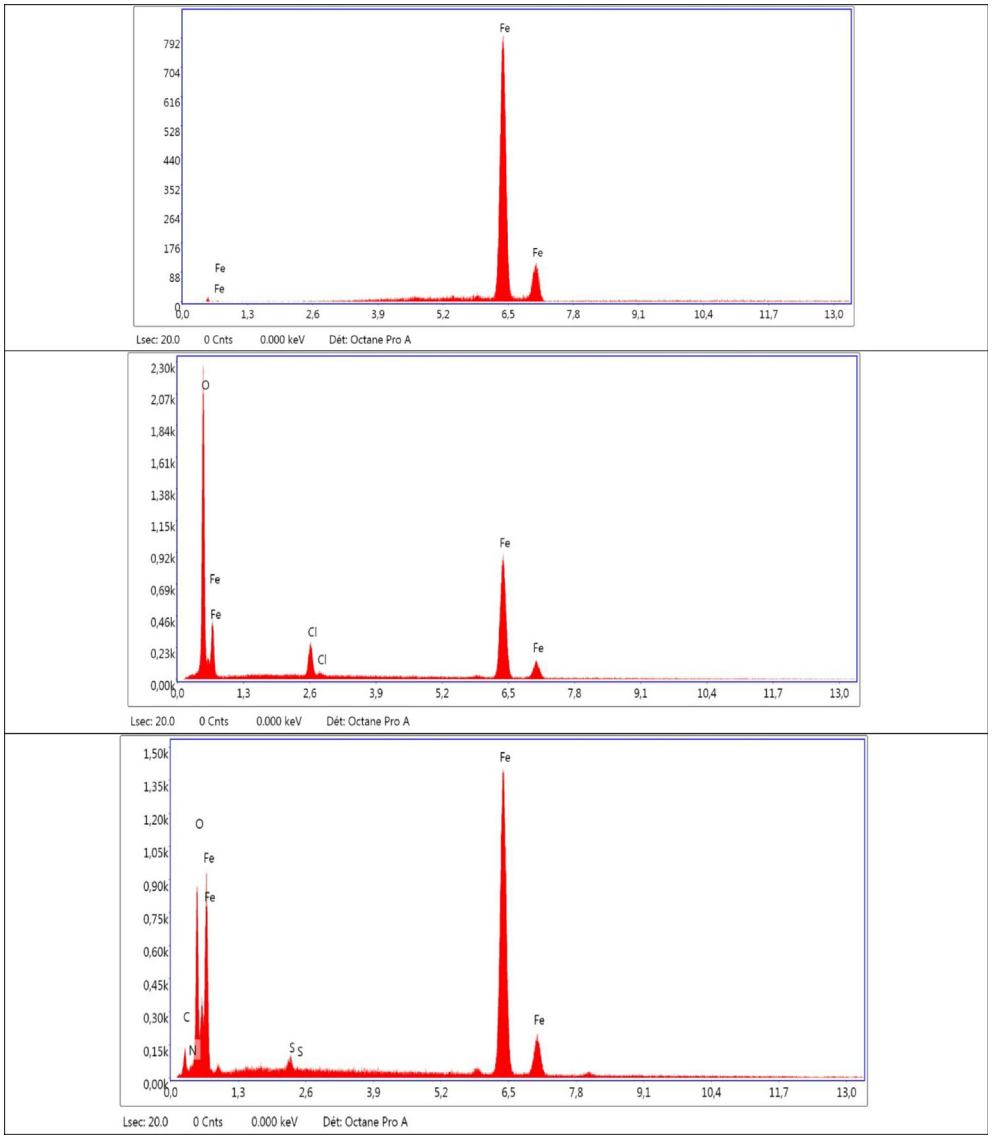

Fig. 14 EDS spectra of mild steel surface: (a) fresh polished; (b and c) are corrosion in 1MHCl without and with 200 ppm DHATSC at room temperature, respectively.

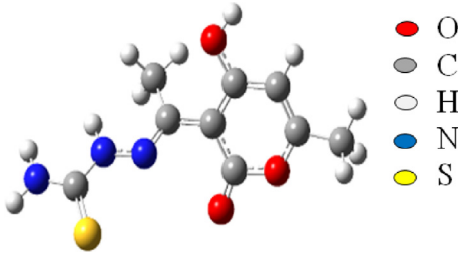

Fig. 15 Optimized structure of DHATSC obtained at B3LYP/6-31G(d) level in DMSO.

Table 7 Calculated molecular descriptors.

MolecularDescriptors	Vacuum	DMSO
α_{Tot} (Bohr^3)	147.96	203.28
E_{HOMO} (eV)	− 5.445	− 5.922
E_{LUMO} (eV)	− 1.401	− 1.551
ΔE_{gap}(eV)	4.044	4.371
E (u.a)	− 1137.676	− 1137.716

electrophilic attack on a site. The highest Fukui function value is attributed to the most reactive of sites. For the Fukui function f_k, which is to the k-site of a molecule, Yang and Mortier presented the condensed form of Fukui functions in a molecule with N electrons. (Aouniti et al., 2016).

$$f_k^+ = [q_k(N+1) - q_k(N)] \tag{19}$$

$$f_k^- = [q_k(N) - q_k(N-1)] (\text{For an electrophilic attack}) \tag{20}$$

$$f_k^0 = \frac{[q_k(N+1) - q_k(N-1)]}{2} (\text{For a radical attack}) \tag{21}$$

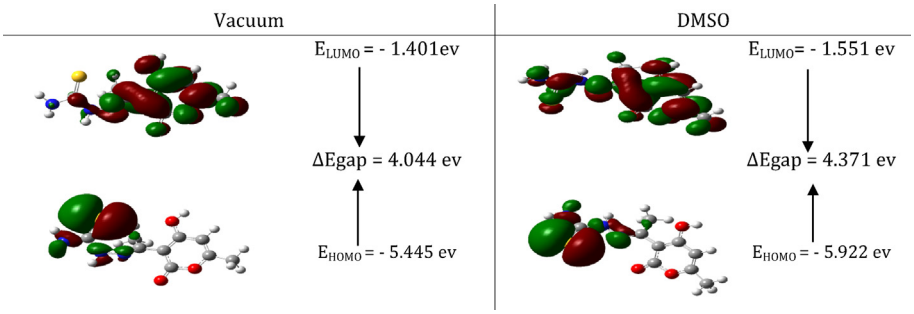

Fig. 16 HOMO and LUMO molecular orbitals of DHATSC in vacuum and DMSO.

Table 8 Equations of global reactivity parameters.

electronegativity	$\chi = -(E_{HOMO} + E_{LUMO}) / 2$
Electronic chemical potential	$\mu = -\chi = (E_{HOMO} + E_{LUMO}) / 2$
chemical hardness	$\eta = (E_{LUMO} - E_{HOMO}) / 2$
electrophilicity index	$\omega = \mu^2 / 2\eta$
molecular softness	$S = 1 / \eta$

$q_k(N)$, $q_k(N + 1)$, and $q_k(N - 1)$ are, respectively, the electron population of atom k in the neutral molecule, in the anion form of the molecule, and the cation form of the molecule. A large value of the Fukui index was found to mean significant site reactivity (Tezcan et al., 2018).

Table 9 Calculated values of (DHATSC) 's reactivity descriptors by B3LYP / 6-31G (d,p) method.

Vacuum					DMSO				
η	s	μ	χ	ω	η	s	μ	χ	ω
2.022	0.4945	− 3.423	3.423	2.897	2.186	0.4576	−3.737	3.737	3.194

Table 10 Parameter of local reactivity of the studied molecule.

atom	f^-	f^+	ω^+
C1	0	0	0
C2	0	0	0
3	0	0	0
C4	0	0	0
C5	0.0001	0.0004	0.0003
C6	0.0001	0	0
C7	0	0	0
O8	0	0	0
C9	0.0003	0.0007	0.0005
O10	0	0	0
C11	0	0.0001	0
N12	0.0007	0.0003	0.0002
N13	0.0112	0.0127	0.0093
C14	0.0764	**0.6611**	**0.4843**
N15	0.0096	0.0124	0.0091
S16	**0.8932**	0.3122	0.2288
H17	0	0	0
H18	0	0	0
H19	0	0	0
H20	0	0	0
H21	0	0	0
H22	0.0001	0	0
H23	0	0	0
H24	0	0	0
H25	0	0	0
H26	0.0006	0	0
H27	0.0076	0	0

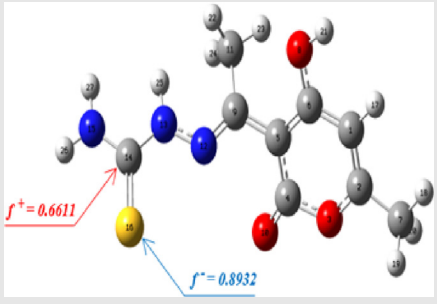

Table 11 Major infrared bands used in experiments (Exp) and theory (Theo) (cm^{-1}).

Bond	Exp	Theo	Δν
NH	3300	3210	− 90
NH_2	3100	3115	15
C = N	1600	1628	28
C = C aromatique	1400	1405	5
C = S	1250	1262	12

Local electrophilicity

The local electrophilicity, ω_k^+(Muthukrishnan et al., 2017) is defined by: $\omega_k^+ = \omega f^+$

The ω is the global electrophilicity index, and f + is the electrophilic Fukui index. The Fukui and local electrophilicity indices results are shown in Table 10. According to the values of f^+ and ω^+, The results of this investigation revealed that the carbon atom (C14) has the largest value. Therefore, it is the most susceptible to attack by a nucleophilic reagent. It is also noted that the sulfur atom (S16) has the highest value of f, which supports that this atom is susceptible to electrophilic attack.

3.11.4. Vibrational study

Vibrational motion is one of three main modes of molecular movement: translational and rotational. It is a periodic motion when one or more atoms move relative to each other in the molecule. The vibrational spectra are coordinated with quantum chemistry calculations to understand the compound's fundamental vibration mode. This work used B3LYP/6-31G(d) to calculate the vibration frequencies. The principal IR bands are listed in Table 11.

Results from this investigation show that this strategy is consistent with previous experience.

3.11.5. Molecular electrostatic potential (MESP)

This map's red and blue areas indicate regions with high and low MESP potential. Green represents a potential between red and blue (red and dark blue). Thus, the electrostatic potential may be ranked as follows: (red > orange > yellow > green > blue). In Fig. 17, the orange area represents the sulfur atom being attacked by an electrophile. At the same time, the green area represents the

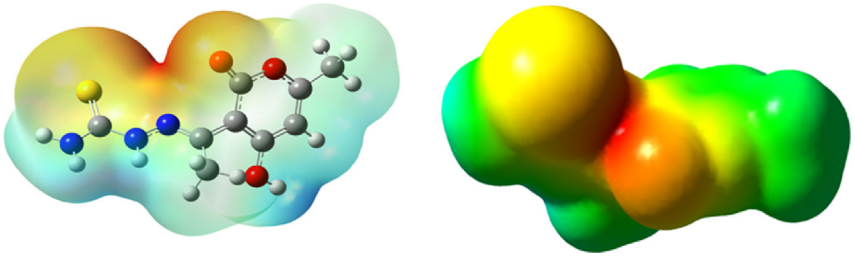

Fig. 17 MESP of the DHATSC: Carbon (gray), Nitrogen (Blue); O (red), H (white), Sulfur (yellow).

Table 12 MCS results. (energies are in kcal/mol).

Energy (kcal mol^{-1})	Total	**12.426**
	Adsorption	$-2.183\ 10^4$
	Rigid adsorption	−18.761
	Deformation	$-2.181\ 10^4$
	DHASC:	$-1.092\ 10^4$
	Hydronium:	$-1.028\ 10^3$
	H_2O:	−9.274
	Cl^-:	−0.564

$\frac{dE_{ad}}{dN_i}$

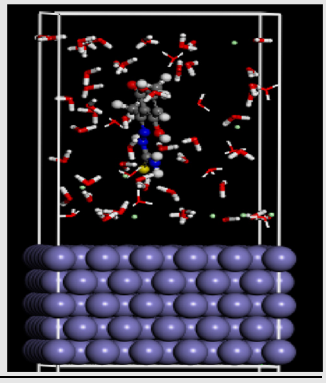

carbon and hydrogen atoms that are also being attacked (Abuelela et al., 2021).

3.12. Monte-carlo simulations (MCS)

Table 12 depicts DHATSC adsorption at maximum efficiency on the Fe (1 1 0) surface and details the computed descriptors in both water and hydrochloric acid solution.

The inhibitor is vertically adsorbing onto the iron (1 1 0) surface. The fact that DHATSC has a negative value for its adsorption energy in the acidic aqueous solution shows that the adsorption of the compound onto the iron surface is a spontaneous and exothermic process. The adsorption energy's absolute value correlates with the adsorption phenotype (Ferkous et al., 2020; Boulechfar et al., 2021; Sedik et al., 2022). The absolute value of $\frac{dE_{ad}}{dN_i}$ is indicative of the stability of the adsorption system, and it increases as inhibitor-Fe (1 1 0) contacts get stronger. Therefore, corrosion inhibition is more effective now. This research shows iron is more difficult to remove than water and Cl^-.

4. Conclusion

Electrochemical testing has confirmed the high efficiency of the recently synthesized Schiff base, DHATSC, in inhibiting the corrosion of XC38 mild steel in 1 M HCl. The inhibition efficiency reached 94.22% at a concentration of 200 ppm and improved with increasing concentration. Polarization experiments demonstrated that the inhibitor exhibits a mixed inhibition behavior. Its primary mechanism of corrosion prevention involves adsorption onto the metal surface, following the Langmuir thermodynamic model. This adsorption process delays both the anodic metal dissolution and cathodic reactive processes.

The validity of these experimental findings is supported by density-functional-theory-based quantum chemistry results, which further contribute to the understanding of corrosion inhibitors. These results highlight a positive correlation between the chemical structure of the inhibitor and its inhibitory effectiveness. The smallest gap value was observed for the molecule examined in a vacuum environment, indicating higher reactivity and lower stability.

In contrast, the molecule was found to be more stable and less reactive in the presence of dimethyl sulfoxide (DMSO), as evidenced by its lower total energy (E) in that environment. Analysis of the molecular orbitals at the frontier reveals the presence of the LUMO orbital throughout the molecule in the DMSO environment. Additionally, the lowest hardness value observed for the molecule in a vacuum suggests reduced stability and increased reactivity.

Declaration of Competing Interest

The authors declare that they have no known competing financial interests or personal relationships that could have appeared to influence the work reported in this paper.

Acknowledgments

The authors express their gratitude for the support provided by the Ministry of Higher Education and Scientific Research, Laboratoire de Géniemécanique et Matériaux, Faculté de Technologie, University 20 Août 1955-Skikda, Skikda, 21000, Algeria, as well as the Directorate General for Scientific Research and Technological Development (DGRSDT), Algeria. The authors are thankful to the Researchers Supporting Project (RSP2023R113), King Saud University, Riyadh, Saudi Arabia.

References

Abd El-Lateef, H.M., Abo-Riya, M.A., Tantawy, A.H., 2016. Empirical and quantum chemical studies on the corrosion inhibition performance of some novel synthesized cationic gemini surfactants on carbon steel pipelines in acid pickling processes. Corros. Sci. 108, 94–110.

Abd El-Lateef, H.M., Soliman, K.A., Tantawy, A.H., 2017. Novel synthesized Schiff Base-based cationic gemini surfactants: Electrochemical investigation, theoretical modeling, and applicability as biodegradable inhibitors for mild steel against acidic corrosion. J. Mol. Liq. 232, 478–498.

Abd-ElHamid, A. et al, 2023. synthesis of gemini cationic surfactants-based pyridine Schiff base for steel corrosion and sulfate-reducing bacteria mitigation. J. Mol. Liq. 369, 120890.

Abdelsalam, M.M. et al, 2022. Green synthesis, electrochemical, and DFT studies on the corrosion inhibition of steel by some novel triazole Schiff base derivatives in hydrochloric acid solution. Arab. J. Chem. 15, (1) 103491.

Abuelela, A.M. et al, 2021. Molecular structure and mild steel/HCl corrosion inhibition of 4, 5-Dicyanoimidazole: Vibrational, electrochemical and quantum mechanical calculations. J. Mol. Struct. 1230, 129647.

Al Zoubi, W. et al, 2020. Recent advances in hybrid organic-inorganic materials with spatial architecture for state-of-the-art applications. Prog. Mater Sci. 112, 100663.

Al Zoubi, W. et al, 2021. Toward two-dimensional hybrid organic-inorganic materials based on an I-PE/UHV-PVD system for exceptional corrosion protection. Appl. Mater. Today 24, 101142.

Al Zoubi, W. et al, 2021. Self-assembled molecular network formed by controlling molecular deposition of organic compounds. FlatChem 29, 100270.

Al Zoubi, W., et al., 2020. Freestanding anti-corrosion hybrid materials based on coordination interaction between metal-quinoline compounds and TiO_2-MgO film. Journal of Colloid and Interface Science 565, 86-95. PEO.

Al-Amiery, A. et al, 2020. Quantum chemical elucidation on corrosion inhibition efficiency of Schiff base: DFT investigations supported by weight loss and SEM techniques. Int. J. Low-Carbon Technol. 15 (2), 202–209.

Al-Gorair, A.S. et al, 2023. Experimental and theoretical studies on the corrosion inhibition on the surface of C-steel in hydrochloric acid solutions using N1, $N^{1'}$-(ethane-1, 2-diyl) bis (N^2-(4-(di-methylamino) benzylidene) ethane-1, 2-diamine). Mater. Chem. Phys. 127351

AltunbaşŞahin, E. et al, 2020. Inhibitive effect of 4-amino-N-benzylidene-benzamide Schiff base on mild steel corrosion in HCl solution. J. Adhes. Sci. Technol. 34 (2), 135–152.

Aouniti, A. et al, 2016. Schiff's base derived from 2-acetyl thiophene as corrosion inhibitor of steel in acidic medium. J. Taibah Univ. Sci. 10 (5), 774–785.

Arjomandi, J. et al, 2018. inhibition of corrosion of aluminum in alkaline solution by a novel azo-Schiff base: Experiment and theory. J. Alloy. Compd. 746, 185–193.

Ashassi-Sorkhabi, H. et al, 2005. Corrosion inhibition of mild steel by some Schiff base compounds in hydrochloric acid. Appl. Surf. Sci. 239 (2), 154–164.

Aytac, A., Özmen, Ü., Kabasakaloğlu, M., 2005. Investigation of some Schiff bases as acidic corrosion of alloy AA3102. Mater. Chem. Phys. 89 (1), 176–181.

Azooz, R. and Kamal, S. 2019. Corrosion and corrosion inhibition of mild steel in Red Sea Water by EDTA. J Material Sci Eng, 8(517), 2169-0022.1000517.

Bedair, M. et al, 2017. Synthesis, electrochemical and quantum chemical studies of some prepared surfactants based on azodye and Schiff base as corrosion inhibitors for steel in acid medium. Corros. Sci. 128, 54–72.

Behloul, H. et al, 2022. New insights on the adsorption of CI-Reactive Red 141 dye using activated carbon prepared from the ZnCl2-treated waste cotton fibers: Statistical physics, DFT, COSMO-RS, and AIM studies. J. Mol. Liq. 364, 119956.

Belakhdar, A. et al, 2020. Computational and experimental studies on the efficiency of Rosmarinus officinalis polyphenols as green corrosion inhibitors for XC48 steel in acidic medium. Colloids Surf A Physicochem Eng Asp 606, 125458.

Belakhdar, A. et al, 2020. Corrosion inhibition performance of Rosmarinus officinalis methanolic extract on carbon steel XC48 in acidic medium (2M HCl). Materials and Biomaterials Science 3 (2), 046–053.

Belakhdar, A. et al. 2021. Thermodynamic and Electrochemical Studies of Corrosion Inhibition of Carbon Steel by Rosmarinus Officinalis Extract in Acid Medium. in Recent Advances in Environmental Science from the Euro-Mediterranean and Surrounding Regions (2nd Edition) Proceedings of 2nd Euro-Mediterranean Conference for Environmental Integration (EMCEI-2), Tunisia 2019. 2021. Springer.

Boukerche, S. et al, 2019. Multilayered ZnO/TiO_2 nanostructures as efficient corrosion protection for stainless steel 304. Mater. Res. Express 6, (5) 055052.

Boulechfar, C. et al, 2021. DFT/molecular scale, MD simulation and assessment of the eco-friendly anti-corrosion performance of a novel Schiff base on XC38 carbon steel in acidic medium. J. Mol. Liq. 344, 117874.

Boulechfar, C. et al, 2023. Synthesis, electrochemical, and quantum chemical studies of some metal complexes: Mn (II), Co (II), and Zn (II) with 2-furaldehyde semicarbazone. J. Mol. Struct. 1271, 134007.

Boulechfar, C., Ferkous, H., Delimi, A., Berredjem, M., Kahlouche, A., Madaci, A., Benguerba, Y., 2023. Corrosion inhibition of Schiff base and their metal complexes with [Mn (II), Co (II) and Zn (II)]: Experimental and quantum chemical studies. J. Mol. Liq. 378, 121637.

Bououden, W. et al, 2021. Surface adsorption of Crizotinib on carbon and boron nitride nanotubes as Anti-Cancer drug Carriers: COSMO-RS and DFT molecular insights. J. Mol. Liq. 338, 116666.

Chugh, B. et al, 2020. Relation of degree of substitution and metal protecting ability of cinnamaldehyde modified chitosan. Carbohydr. Polym. 234, 115945.

Chugh, B. et al, 2020. A comprehensive study about anti-corrosion behaviour of pyrazine carbohydrazide: Gravimetric, electrochemical, surface and theoretical study. J. Mol. Liq. 299, 112160.

de Britto Policarpi, E., Spinelli, A., 2020. Application of Hymenaeastigonocarpa fruit shell extract as eco-friendly corrosion inhibitor for steel in sulfuric acid. J. Taiwan Inst. Chem. Eng. 116, 215–222.

Delimi, A. et al, 2022. Corrosion protection performance of silicon-based coatings on carbon steel in NaCl solution: a theoretical and experimental assessment of the effect of plasma-enhanced chemical vapor deposition pretreatment. RSC Adv. 12 (24), 15601–15612.

Djellali, S., et al. 2021. Efficiency of Alkaloids Crude Extract of Cinnamomum Zeylanicum as Corrosion Inhibitor of Mild Steel in Sulfuric Acid Solution. in Recent Advances in Environmental Science from the Euro-Mediterranean and Surrounding Regions (2nd Edition) Proceedings of 2nd Euro-Mediterranean Conference for Environmental Integration (EMCEI-2), Tunisia 2019. Springer.

Ehteshamzade, M., Shahrabi, T., Hosseini, M., 2006. Inhibition of copper corrosion by self-assembled films of new Schiff bases and their modification with alkanethiols in aqueous medium. Appl. Surf. Sci. 252 (8), 2949–2959.

El Batouti, M. et al, 2021. Novel heterogeneous cellulose-based ion-exchange membranes for electrodialysis. Polym. Bull. 1–25.

El Batouti, M. et al, 2023. Preparation and characterization of new optical active charge transfer complexes for mitigation climate changes. Inorg. Chem. Commun. 152, 110648.

Ferkous, H. et al, 2017. Green Corrosion Inhibitor for Carbon Steel in 1 M HCl: A Comparative Study of Polysaccharides Extracted from Prickly Pear Nopals of Opuntia Ficus-Indica (Peel and Pulp). Euro-Mediterranean Conference for Environmental Integration. Springer.

Ferkous, H. et al, 2020. Corrosion inhibition of mild steel by 2-(2-methoxy benzylidene) hydrazine-1-carbothioamide in hydrochloric acid solution: Experimental measurements and quantum chemical calculations. J. Mol. Liq. 307, 112957.

Ferkous, H. et al, 2022. Electrochemical and Computational Approaches of Polymer Coating on Carbon Steel X52 in Different Soil Extracts. Polymers 14 (16), 3288.

Ferkous, H., et al. 2018. Electrochemical and Surface Morphological Studies of a Carbon Steel Corrosion by Natural Product in Acidic Solution. in Recent Advances in Environmental Science from the Euro-Mediterranean and Surrounding Regions: Proceedings of Euro-Mediterranean Conference for Environmental Integration (EMCEI-1), Tunisia 2017. Springer.

Ferkous, H., et al. Electrochemical Impedance Spectroscopy and Adsorption Study of Carbon Steel in 1 M HCl Solution Containing 2-(2-Methoxybenzylidene) Hydrazine-1-Carbothioamide. in Recent Advances in Environmental Science from the Euro-Mediterranean and Surrounding Regions (2nd Edition) Proceedings of 2nd Euro-Mediterranean Conference for Environmental Integration (EMCEI-2), Tunisia 2019. Springer.

Ferkous, H., et al. 2021. 2-(2-Methoxybenzylidene) Hydrazine-1-Carbothioamide as Efficient Organic Inhibitor for Mild Steel in Hydrochloric Acid Solution. In Recent Advances in Environmental Science from the Euro-Mediterranean and Surrounding Regions (2nd Edition) Proceedings of 2nd Euro-Mediterranean Conference for Environmental Integration (EMCEI-2), Tunisia 2019. Springer.

Frenkel, D., Smit, B., Ratner, M.A., 1996. Understanding molecular simulation: from algorithms to applications. Academic Press San Diego.

Haque, J. et al, 2020. Polar group substituted imidazolium zwitterions as eco-friendly corrosion inhibitors for mild steel in acid solution. Corros. Sci. 172, 108665.

Heakal, F.-E.-T. et al, 2018. Performance of Centaurea cyanus aqueous extract towards corrosion mitigation of carbon steel in saline formation water. Desalination 425, 111–122.

Hossain, M.S. et al, 2017. Synthesis, spectral and thermal characterization of Cu (II) complexes with two new Schiff base ligand towards potential biological application. Der ChemicaSinica 8 (3), 380–392.

Hsissou, R. et al, 2021. insight into the corrosion inhibition of novel macromolecular epoxy resin as highly efficient inhibitor for carbon steel in acidic mediums: Synthesis, characterization, electrochemical techniques, AFM/UV–Visible and computational investigations. J. Mol. Liq. 337, 116492.

Ibrahim, M.M. et al, 2016. Schiff′ s Bases and Their Metal Complexes as Corrosion Inhibitors for Aluminum Alloys in Corrosive Media. ChemInform 47 (21), p. no-no.

Issaadi, S., Douadi, T., Chafaa, S., 2014. Adsorption and inhibitive properties of a new heterocyclic furan Schiff base on corrosion of copper in HCl 1 M: experimental and theoretical investigation. Appl. Surf. Sci. 316, 582–589.

Kahlouche, A. et al, 2022. Molecular insights through the experimental and theoretical study of the anti-corrosion power of a new eco-friendly Cytisusmultiflorus flowers extract in a 1 M sulfuric acid. J. Mol. Liq. 347, 118397.

Kaya, F., Solmaz, R., Geçibesler, İ.H., 2023. Adsorption and Corrosion Inhibition Capability of Rheum Ribes Root Extract (Işgın) for Mild Steel Protection in Acidic Medium: A Comprehensive Electrochemical, Surface Characterization, Synergistic Inhibition Effect, and Stability Study. J. Mol. Liq. 121219

Khamis, A., Saleh, M., Awad, M., 2013. Synergistic inhibitor effect of cetylpyridinium chloride and other halides on the corrosion of mild steel in 0.5 M H_2SO_4. Corros. Sci. 66, 343–349.

Leontie, L. et al, 2018. Electric and optical properties of some new functional lower-rim-substituted calixarene derivatives in thin films. Appl. Phys. A 124, 1–12.

Li, X.-L. et al, 2022. 2-Pyridinecarboxaldehyde-based Schiff base as an effective corrosion inhibitor for mild steel in HCl medium: Experimental and computational studies. J. Mol. Liq. 345, 117032.

Liang, C. et al, 2019. synthesis of 2-amino fluorene bis-Schiff base and corrosion inhibition performance for carbon steel in HCl. J. Mol. Liq. 277, 330–340.

Liu, X. et al, 2018. Multi-dentate unsymmetrically-substituted Schiff bases and their metal complexes: Synthesis, functional materials properties, and applications to catalysis. Coord. Chem. Rev. 357, 144–172.

Messali, M. et al, 2018. A new Schiff base derivative as an effective corrosion inhibitor for mild steel in acidic media: Experimental and computer simulations studies. J. Mol. Struct. 1168, 39–48.

Miralrio, A., Espinoza Vázquez, A., 2020. Plant extracts as green corrosion inhibitors for different metal surfaces and corrosive media: a review. Processes 8 (8), 942.

Mishra, M. et al, 2015. Versatile coordination behaviour of a multi-dentate Schiff base with manganese (II), copper (II) and zinc (II) ions and their corrosion inhibition study. InorganicaChimica Acta 425, 36–45.

Mishra, M. et al, 2015. synthesis, characterization and corrosion inhibition property of nickel (II) and copper (II) complexes with some acyl hydrazine Schiff bases. Polyhedron 89, 29–38.

Muthukrishnan, P., Jeyaprabha, B., Prakash, P., 2017. Adsorption and corrosion inhibiting behavior of Lanneacoromandelica leaf extract on mild steel corrosion. Arab. J. Chem. 10, S2343–S2354.

Naik, U. et al, 2016. Electrochemical and theoretical investigation of the inhibitory effect of two Schiff bases of benzaldehyde for the corrosion of aluminum in hydrochloric acid. J. Mol. Struct. 1125, 63–72.

Nakhli, A. et al, 2020. Molecular insights through computational modeling of methylene blue adsorption onto low-cost adsorbents derived from natural materials: A multimodel's approach. Comput. Chem. Eng. 140, 106965.

Pearson, R.G., 1992. The electronic chemical potential, and chemical hardness. J. Mol. Struct. (Thoechem) 255, 261–270.

Prajila, M., Ammal, P.R., Joseph, A., 2018. Comparative studies on the corrosion inhibition characteristics of three different triazine-based Schiff's bases, HMMT, DHMMT, and MHMMT, for mild steel exposed in sulfuric acid. Egypt. J. Pet. 27 (4), 467–475.

Radjai, M., et al. Methanolic Extract of Artemisia Herba Alba as Eco-Friendly Inhibitor of Carbon Steel Corrosion in 1M HCl Media. in Recent Advances in Environmental Science from the Euro-Mediterranean and Surrounding Regions: Proceedings of Euro-Mediterranean Conference for Environmental Integration (EMCEI-1), Tunisia 2017. Springer.

Şafak, S. et al, 2012. Schiff bases as corrosion inhibitor for aluminum in HCl solution. Corros. Sci. 54, 251–259.

Sahu, R., Thakur, D., 2012. Schiff base: An overview of its medicinal chemistry potential for new drug molecules. Inter. J. Pharm. Sci. Nanotechnology 5 (3), 1757–1764.

Saifi et al, 2019. Electrochemical behavior investigation of cysteine on nickel corrosion in acidic medium. J. Fail. Anal. Prev. 19, 1597–1606.

Sakthivel, A. et al, 2020. Recent advances in Schiff base metal complexes derived from 4-amino antipyrine derivatives and their potential applications. J. Mol. Struct. 1222, 128885.

Sedik, A. et al, 2014. Synergistic Effect of L-Methionine and KI on Copper Corrosion Inhibition in HNO_3 (1M). Sensors & Transducers 27 (Special Issue).

Sedik, A. et al, 2020. Dardagan Fruit extract as eco-friendly corrosion inhibitor for mild steel in 1 M HCl: Electrochemical and surface morphological studies. J. Taiwan Inst. Chem. Eng. 107, 189–200.

Sedik, A. et al, 2022. Experimental and theoretical insights into copper corrosion inhibition by protonated amino-acids. RSC Adv. 12 (36), 23718–23735.

Sedik, A., Abderrahmane, S., Himour, A., 2011. Cysteine inhibitor effects on copper corrosion in 1 M HNO_3 solution. Sens. Lett. 9 (6), 2219–2222.

Singh, A.K. et al, 2019. Evaluation of the anti-corrosion performance of expired semi-synthetic antibiotic cefdinir for mild steel in 1 M HCl medium: An experimental and theoretical study. Results Phys. 14, 102383.

Singh, A.K., Quraishi, M., Ebenso, E.E., 2011. Inhibitive effect of Cefuroxime on the corrosion of mild steel in hydrochloric acid solution. Int. J. Electrochem. Sci 6, 5676–5688.

Solmaz, R., Altunbaş, E., Kardaş, G., 2011. Adsorption and corrosion inhibition effect of 2-((5-mercapto-1, 3, 4-thiadiazol-2-amino) methyl) phenol Schiff base on mild steel. Mater. Chem. Phys. 125 (3), 796–801.

Solomon, M.M., Umoren, S.A., 2016. In-situ preparation, characterization and anti-corrosion property of polypropylene glycol/silver nanoparticles composite for mild steel corrosion in acid solution. J. Colloid Interface Sci. 462, 29–41.

Srivastava, V. et al, 2017. Amino acid based imidazolium zwitterions as novel and green corrosion inhibitors for mild steel: Experimental, DFT and MD studies. J. Mol. Liq. 244, 340–352.

Suhasaria, A. et al, 2020. Bis-benzothiazoles as efficient corrosion inhibitors for mild steel in aqueous HCl: molecular structure-reactivity correlation study. J. Mol. Liq. 313, 113537.

Sun, H., 1998. Simulation of organic adsorption on metallic materials. J. Phys. Chem. B 102, 7338.

Tezcan, F. et al, 2018. A novel thiophene Schiff base as an efficient corrosion inhibitor for mild steel in 1.0 M HCl: electrochemical and quantum chemical studies. J. Mol. Liq. 269, 398–406.

Verma, C. et al, 2018. Substituents effect on corrosion inhibition performance of organic compounds in aggressive ionic solutions: a review. J. Mol. Liq. 251, 100–118.

Yurt, A., Aykın, Ö., 2011. Diphenolic Schiff bases as corrosion inhibitors for aluminum in 0.1 M HCl: potentiodynamic polarisation and EQCM investigations. Corros. Sci. 53 (11), 3725–3732.

Zerroug, M. et al, 2021. Experimental and theoretical evaluation of the adsorption process of some polyphenols and their corrosion inhibitory properties on mild steel in acidic media. J. Environ. Chem. Eng. 9, (6) 106482.

Zerroug, M., et al. 2018. An AFM Study of the Surface Propriety and Corrosion Inhibition on Carbon Steel in Acidic Media. in Recent Advances in Environmental Science from the Euro-Mediterranean and Surrounding Regions: Proceedings of Euro-Mediterranean Conference for Environmental Integration (EMCEI-1), Tunisia 2017. Springer.

Zhang, J. et al, 2016. inhibition of copper corrosion by the formation of Schiff base self-assembled monolayers. Appl. Surf. Sci. 389, 601–608.